Bulgarian Journal of Physics vol. **48** (2021) 202–224

Image Charges Re-Imagined

H. Alshal[1,2], **T.L. Curtright**[2], **S. Subedi**[2]
[1]Department of Physics, Cairo University, Giza, 12613, Egypt
[2]Department of Physics, University of Miami, Coral Gables, FL 33124-8046, USA

Received *February 21, 2021*

Abstract. We discuss the grounded, equipotential ellipse in two-dimensional electrostatics to illustrate different ways of extending the domain of the potential and placing image charges such that homogeneous boundary conditions are satisfied. In particular, we compare and contrast the Kelvin and Sommerfeld image methods. We present our discussion at a level suitable for use in advanced undergraduate and introductory graduate courses on electrostatics, as a supplement to more traditional material on image methods.

1 Introduction

When a source charge is placed near a real, grounded conductor, electrical charge flows between the ground and the conductor. In the static limit, for an idealized conductor, the resulting induced charge distribution is entirely on the surface of the conductor. In this ideal static situation the *interior* of the conductor is an equipotential containing no charge, and therefore not very interesting. However, for mathematical expediency, in some cases one can easily *imagine* a distribution of charge located entirely *inside* the conductor, instead of on the surface, which gives exactly the same *exterior* effects as the actual surface charge distribution.

All this is well-known, of course, and the subject is almost always discussed in advanced undergraduate or introductory graduate courses, but it may not be fully appreciated that the imagined distribution of charge within the conductor is *not* uniquely determined[1] for the simple reason that the interior of the conductor can be imagined in different ways. So far as physics outside an ideal conductor is concerned, there is a great deal of mathematical freedom to choose the interior of the conductor (i.e. the domain of the image charge) as an extension of the exterior (i.e. the domain of the real source charge) to be almost *any* imagined

[1]In making this statement, we are not comparing apples to oranges. It is well-known that different boundary conditions, such as Dirichlet and Neumann, are handled using different image charges. However, our statement is correct even when the boundary conditions are not different. In this paper, we consider one specific set of mixed homogeneous Dirichlet and Neumann boundary conditions.

manifold, with the only essential restriction being that the image and source domains have in common a boundary, namely, the surface of the ideal conductor.[2]

This somewhat surprising mathematical freedom can be illustrated by a simple example to be discussed here: The grounded two-dimensional (2D) ellipse. Two image methods, established long ago by Thomson (a.k.a. Lord Kelvin) [1] and somewhat later by Sommerfeld [2], will be compared and contrasted. The image domains for these two methods have different geometries, but nevertheless give exactly the same physical results in the source domain. The Kelvin method has the advantage that the Green function [3] is usually easier to extend from the source domain to the image domain. On the other hand, the Sommerfeld method has the advantage that the location of the image is always obvious given the location of the actual source charge. Our discussion is intended for use as a supplement to more traditional approaches to the method of images, or perhaps to motivate and provide guidance for a class project by students who wish to pursue the subject in more depth.

2 Kelvin versus Sommerfeld Images – A Simple Illustration

The simplest example to illustrate the method of images is the electrostatics problem of the grounded plane, or rather, for the purposes of this paper, its 2D analogue, the grounded line. The standard Green function on the entire plane follows from the logarithmic potential [4–6], $-\frac{1}{2\pi}\ln\left(\left|\overrightarrow{r}\right|/R\right)$, which involves an arbitrary scale R. In terms of rectangular Cartesian coordinates on the entire plane, $-\infty < x < +\infty$ and $-\infty < y < +\infty$, with orthogonal unit vectors, $\widehat{x}$ and $\widehat{y}$, and with $\overrightarrow{r} = x\,\widehat{x} + y\,\widehat{y}$, the standard Green function is then

$$g\left(x_1, y_1; x_2, y_2\right) = -\frac{1}{4\pi}\ln\left(\frac{\left(x_1 - x_2\right)^2 + \left(y_1 - y_2\right)^2}{R^2}\right). \tag{1}$$

Here (x_1, y_1) is the "field point" and (x_2, y_2) is the "source point". Note the symmetries $g\left(x_1, y_1; x_2, y_2\right) = g\left(x_2, y_1; x_1, y_2\right) = g\left(x_1, y_2; x_2, y_1\right) = g\left(x_2, y_2; x_1, y_1\right)$. This g is a fundamental solution of the inhomogeneous equation

$$\left(\frac{\partial^2}{\partial x_1^2} + \frac{\partial^2}{\partial y_1^2}\right) g\left(x_1, y_1; x_2, y_2\right) = -\,\delta\left(x_1 - x_2\right)\,\delta\left(y_1 - y_2\right), \tag{2}$$

with a 2D Dirac delta source on the right-hand side (RHS). This Green function is therefore the logarithmic potential produced at the field point by an ideal point charge located at the source point. For a general source charge density on the plane, ρ, an electrostatic potential satisfying

$$\left(\frac{\partial^2}{\partial x^2} + \frac{\partial^2}{\partial y^2}\right)\Phi\left(x, y\right) = -\rho\left(x, y\right), \tag{3}$$

[2]The topology of the extended manifold may also be re-imagined, but here we will not discuss that issue any further.

with some implicit boundary conditions, is then given by

$$\Phi\left(x,y\right)=\int_{-\infty}^{+\infty}dX\int_{-\infty}^{+\infty}dY\ g\left(x,y;X,Y\right)\ \rho\left(X,Y\right). \tag{4}$$

To "ground the line" $y=a$, and obtain a Green function as well as a general potential on the half-plane $y>a$, such that both satisfy homogeneous Dirichlet boundary conditions for $y=a$, it suffices just to replace the Green function g with the linear combination

$$g_o\left(x_1,y_1;x_2,y_2\right)=g\left(x_1,y_1;x_2,y_2\right)-g\left(x_1,2a-y_1;x_2,y_2\right). \tag{5}$$

so that $g_o\left(x_1,a;x_2,y_2\right)=0$. Note that unlike g in (1), g_o also vanishes as $y_1\to\infty$. This result has a well-known interpretation, sometimes appropriately attributed to Kelvin, but most often with no attribution at all. The interpretation follows from noting it is also true that

$$g_o\left(x_1,y_1;x_2,y_2\right)=g\left(x_1,y_1;x_2,y_2\right)-g\left(x_1,y_1;x_2,2a-y_2\right). \tag{6}$$

Thus the first term on the RHS is interpreted as a potential at the field point (x_1,y_1) due to a point charge source at (x_2,y_2) while the second term is interpreted as a potential at the field point due to a negative "mirror image" point charge source at $(x_2,2a-y_2)$, the so-called Kelvin image. In this construction the half-plane $y>a$ has been extended to the full plane, including all $y<a$, to allow placement of the Kelvin image in the "unphysical" region below the grounded line. Consequently, for all $y>a$ the equation (2) holds for g_o as well as for g. The corresponding grounded potential for a general charge density situated in the half-plane $y>a$ is then

$$\Phi\left(x,y\right)=\int_{-\infty}^{+\infty}dX\int_{a}^{+\infty}dY\ g_o\left(x,y;X,Y\right)\ \rho\left(X,Y\right). \tag{7}$$

From (5) it follows immediately that $\Phi\left(x,a\right)=0$. Moreover, the contributions to Φ arising from the two terms in g_o may then be interpreted respectively as due to the real source density $\rho\left(X,Y\right)$ above the grounded line, and an image source density $-\rho\left(X,2a-Y\right)$ below that line. However, there are other ways to visualize the image charges. For example, the Euclidean plane may be *folded* along the grounded line to obtain two copies of the half-plane $y>a$, with the negative image charge now located on the second copy of the half-plane at the *same* position as the source point, namely, (x_2,y_2). This technique of employing a second copy of the physical space is due to Sommerfeld, following in the footsteps of Riemann to construct a branched manifold. The real beauty of Sommerfeld's technique, in principle, is that doubling the physical space *obviously* works to provide the location of the image charges for all homogeneous boundary condition potential problems in any number of dimensions. But let's not get ahead of ourselves.

As it happens, for this particularly simple example, there is essentially *no difference* in the two methods. Mostly this is just because the intrinsic geometry of the folded plane is indistinguishable from that of the unfolded plane. Nevertheless, it is instructive to exhibit analytically the parameterization of the folded space to be able to express the Green function in Sommerfeld's approach. Here this is easily done: Represent the original half-plane by points $(x, y) = (x, a + w)$ for $w > 0$ and the second copy of the half-plane by points $(x, y) = (x, a - w)$ for $w < 0$. (Note that the fold occurs at $w = 0$, hence at $y = a$.) That is to say, the branched, folded plane is represented by the points $(x, y) = (x, a + |w|)$ for $-\infty < w < +\infty$. It is then important to understand that point charges placed at the same x but at different values of w do *not* coincide, even though they may have the same $|w|$. Such points with different w but the same $|w|$ are on opposite branches of the folded, doubled space.

A Green function on both branches of the folded space is now given by

$$g\left(x_1, w_1; x_2, w_2\right) = -\frac{1}{4\pi} \ln\left(\frac{\left(x_1 - x_2\right)^2 + \left(w_1 - w_2\right)^2}{R^2}\right), \tag{8}$$

for $-\infty < x_{1,2} < +\infty$ and $-\infty < w_{1,2} < +\infty$, and it again provides a fundamental solution of

$$\left(\frac{\partial^2}{\partial x_1^2} + \frac{\partial^2}{\partial w_1^2}\right) g\left(x_1, w_1; x_2, w_2\right) = -\,\delta\left(x_1 - x_2\right)\,\delta\left(w_1 - w_2\right). \tag{9}$$

But indeed, for this simple example, this g is *exactly the same expression* as the previous Green function on the unfolded plane. Similarly, grounding the line at $y = a$ is now accomplished by the linear combination

$$g_o\left(x_1, w_1; x_2, w_2\right) = g\left(x_1, w_1; x_2, w_2\right) - g\left(x_1, -w_1; x_2, w_2\right), \tag{10}$$

Moreover, the potential on the half-plane $y > a$, for a general ρ distributed on that same half-plane, with the line $y = a$ grounded, is now

$$\Phi\left(x, w\right) = \int_{-\infty}^{+\infty} dX \int_{0}^{+\infty} dW\; g_o\left(x, w; X, W\right)\; \rho\left(X, W\right), \tag{11}$$

where the field point is $(x, y) = (x, a + w)$ for $w > 0$. The contributions arising from the two terms in g_o may then be interpreted respectively as due to the real source density $\rho\left(X, W\right)$ above the grounded line, and the image source density $-\rho\left(X, -W\right)$ also above the grounded line, but *on the opposite branch of the folded plane*.

We wish to emphasize that the grounded line example is unique in its simplicity as a 2D image system, since other examples have very different geometries for their Kelvin and Sommerfeld image domains. We consider next a situation where the alternative geometries of the combined source and image manifolds for the Kelvin and Sommerfeld approaches are not so simply related, namely, the grounded 2D ellipse.

3 Green Functions for a 2D Ellipse

In this section we construct the electrostatic Green function for a grounded ellipse in two spatial dimensions, i.e. a plane, where the source point lies on the plane outside the ellipse.

This problem is nicely solved using complex analysis, as has been known since the 19th century (e.g. see the literature cited in [7]). However, here we use real variables in anticipation of higher dimensional situations. (Appendices Appendix A: and Appendix B: discuss connections between our choice of real variables and those of the conventional complex plane.) In terms of real elliptic coordinates for the xy-plane[3] as illustrated in Figure 1,

$$x = a\cosh u\cos v, y = a\sinh u\sin v, 0 \leq u \leq \infty, 0 \leq v \leq 2\pi. \tag{12}$$

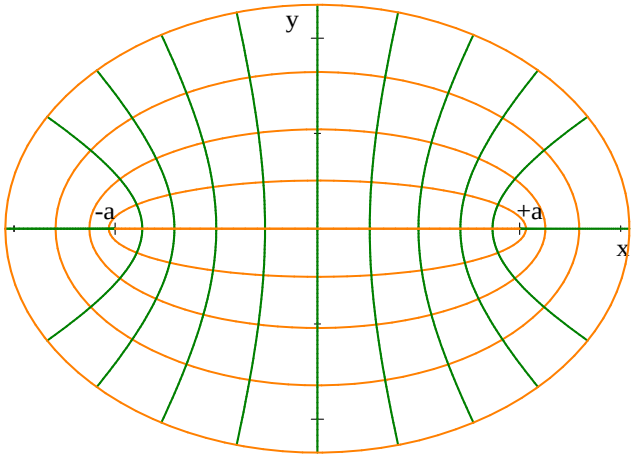

Figure 1. Elliptic coordinates (12) with constant u curves in orange, and constant v curves in green.

Remarkably, the standard method to construct the 2D Laplacian Green function as sums of harmonic functions (e.g. see [6, 8]) now leads to an unusual form for the result.

$$G\left(u_1, v_1; u_2, v_2\right) = -\frac{1}{4\pi}\left|u_1 - u_2\right| \\ -\frac{1}{4\pi}\ln\left(1 + e^{-2|u_1-u_2|} - 2e^{-|u_1-u_2|}\cos\left(v_1 - v_2\right)\right). \tag{13}$$

[3] The straight line segment connecting the two elliptical foci on the x-axis at $\pm a$ is covered twice using real elliptic coordinates.

Note that in addition to being 2π-periodic[4] in each of the vs this Green function also has the following symmetries similar to those for g above: $G\left(u_1, v_1; u_2, v_2\right) = G\left(u_2, v_1; u_1, v_2\right) = G\left(u_1, v_2; u_2, v_1\right) = G\left(u_2, v_2; u_1, v_1\right)$. By construction, G is again a fundamental solution of the equation[5]

$$\left(\frac{\partial^2}{\partial u_1^2} + \frac{\partial^2}{\partial v_1^2}\right) G\left(u_1, v_1; u_2, v_2\right) = -\,\delta\left(u_1 - u_2\right)\,\delta\left(v_1 - v_2\right), \tag{14}$$

and it incorporates some implicit boundary conditions. For example, all v dependence in G is exponentially suppressed as either u_1 or u_2 become infinite, with the other u fixed. It is interesting to compare (13) to the more well-known form given in (1). This is easily done using the elementary identity

$$\begin{aligned}&\left(\cosh u_1 \cos v_1 - \cosh u_2 \cos v_2\right)^2 + \left(\sinh u_1 \sin v_1 - \sinh u_2 \sin v_2\right)^2 \\ &= \left(\cosh\left(u_1 - u_2\right) - \cos\left(v_1 - v_2\right)\right)\left(\cosh\left(u_1 + u_2\right) - \cos\left(v_1 + v_2\right)\right).\end{aligned} \tag{15}$$

Upon converting $x_{1,2}$ and $y_{1,2}$ to the elliptic coordinates in (12), this identity gives

$$\begin{aligned} g(x_1, y_1; x_2, y_2) &= -\frac{1}{4\pi} \ln\Big(\frac{a^2}{R^2}(\cosh u_1 \cos v_1 - \cosh u_2 \cos v_2)^2 \\ &\quad + (\sinh u_1 \sin v_1 - \sinh u_2 \sin v_2)^2\Big) \\ &= -\frac{1}{4\pi} \ln\left(2\cosh(u_1 - u_2) - 2\cos(v_1 - v_2)\right) \\ &\quad - \frac{1}{4\pi} \ln\Big(\frac{a^2}{2R^2}\left(\cosh(u_1 + u_2) - \cos(v_1 + v_2)\right)\Big) \\ &= G(u_1, v_1; u_2, v_2) - \frac{1}{4\pi} \ln\Big(\frac{a^2}{2R^2}\left(\cosh(u_1 + u_2) - \cos(v_1 + v_2)\right)\Big) \end{aligned} \tag{16}$$

Therefore, for $u_1 + u_2 \neq 0$ and real $v_1 + v_2$, the difference $g - G$ is a non-singular, harmonic function, as must be the case for two fundamental solutions of (14).

[4] As a consequence of this 2π-periodicity, G could also be interpreted as the potential for an infinite line of uniformly spaced point charges on the uv-plane, i.e. on the covering space for the (u, v) cylinder defined by (12). In that case the $\delta\left(v_1 - v_2\right)$ on the RHS of (14) would be a Dirac comb. However, here we are interested in only one copy of the cylinder, so this interpretation is not relevant to the problem at hand.

[5] At first sight it may be surprising that (14) is the equation to be solved, since the elliptic coordinates defined in (12) involve a non-trivial metric. However, the metric dependence factors out of the invariant Laplacian expressed in terms of those elliptic coordinates. Thus, the covariant equation for the Green function, namely, $\frac{1}{\sqrt{g}}\,\partial_\mu\left(\sqrt{g}\,g^{\mu\nu}\partial_\nu G\right) = -\frac{1}{\sqrt{g}}\,\delta\left(u_1 - u_2\right)\,\delta\left(v_1 - v_2\right)$, simply reduces to (14).

3.1 The Kelvin image method

Characterized generally, albeit somewhat vaguely, the Kelvin image method makes use of both the interior *and* the exterior of the ellipse, placing source and image charges in opposite regions on the plane so as to satisfy boundary conditions. In the elliptic coordinate frame, an obvious construction of a Green function for a grounded ellipse is given by the linear combination

$$G_o\left(u_1, v_1; u_2, v_2\right) = G\left(u_1, v_1; u_2, v_2\right) - G\left(u_1, v_1; 2U - u_2, v_2\right) \tag{17}$$

where the grounded ellipse consists of points given by (U, v) for a fixed U and $0 \leq v \leq 2\pi$. This Green function satisfies homogeneous Dirichlet boundary conditions on the ellipse, i.e. $G_o\left(u_1, v_1; U, v_2\right) = 0$. From the symmetry of G it is also true that $G_o\left(U, v_1; u_2, v_2\right) = 0$ for all v_1, u_2, and v_2. On the other hand, as constructed G_o satisfies homogeneous Neumann boundary conditions at infinity, i.e. $\lim_{r\to\infty} \overrightarrow{\nabla} G_o = 0$. Some contour plots of G_o are given in Appendix Appendix C:, for $U = 1$ and some representative field points.

For a general distribution of source charge either inside or outside the grounded ellipse, as given by $\rho\left(u, v\right)$, the solution of

$$\left(\frac{\partial^2}{\partial u^2} + \frac{\partial^2}{\partial v^2}\right) \Phi\left(u, v\right) = -k\, \rho\left(u, v\right) \tag{18}$$

is then reduced to the evaluation of an integral involving G_o and ρ. In particular, for field points and actual sources outside the grounded ellipse, the electric potential is

$$\Phi\left(u_1, v_1\right) = k \int\limits_{U < u_2 \leq \infty} \int\limits_{0 \leq v_2 \leq 2\pi} G_o\left(u_1, v_1; u_2, v_2\right) \rho\left(u_2, v_2\right) du_2 dv_2. \tag{19}$$

Here we have introduced k as a 2D analogue of the Coulomb constant.

The first G in (17) is universally interpreted as a potential at field point (u_1, v_1) produced by a positive unit point source at location (u_2, v_2). The second G in (17) is similarly interpreted as a potential at field point (u_1, v_1) produced by another point-like, but in this case negative, *Kelvin image* at location $(2U - u_2, v_2)$. However, for the grounded ellipse construction in (17) there are some interesting – perhaps unexpected – features.

For both field and source points inside the grounded ellipse, such that $0 \leq u_1, u_2 \leq U$, the Kelvin image is always outside that ellipse with $U \leq 2U - u_2 \leq 2U$, and therefore the image is *never* located at infinity[6] as long as both $a \neq 0$ and $U \neq \infty$. That is to say, to implement an interior Green function construction inside a grounded ellipse at $u = U$, it suffices to use a single point-like

[6]This differs from a grounded circle in 2D (or sphere in 3D) where the image is located by inversion and *can* move toward infinity as the source moves toward the center of the circle (or sphere). The limit where the ellipse becomes a circle of radius R is achieved here by

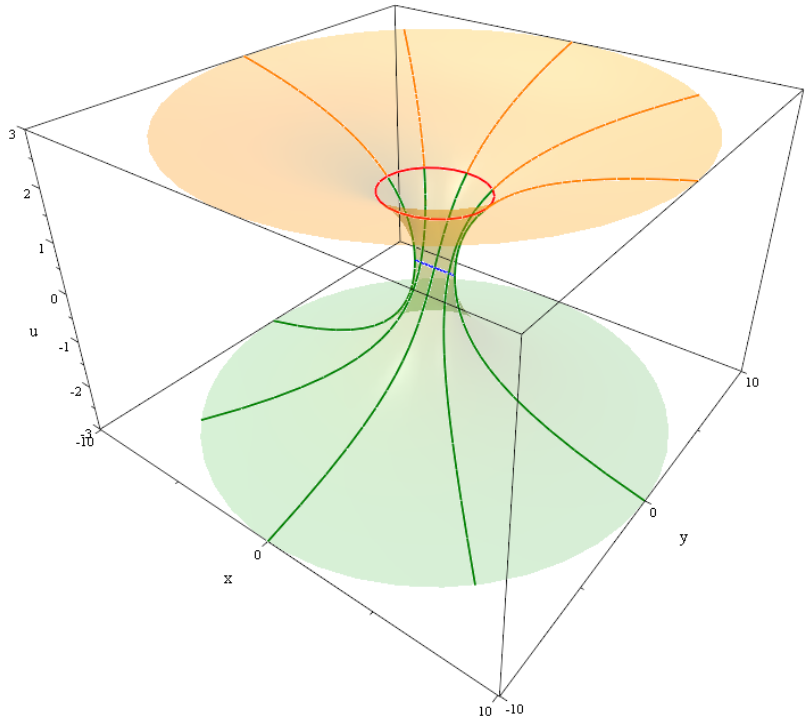

Figure 2. Representative "trajectories"for exterior sources (orange) and their Kelvin images (green) for a grounded ellipse (red) with $U = 3/2$. As a point source moves away from the red ellipse along one of the orange curves, its image moves away from the red ellipse along a corresponding extension shown as a green curve. A straight line segment between the foci is shown in blue.

Kelvin image that lies between the confocal ellipses at $u = U$ and $u = 2U$. As expected, the image is outside the source domain defined by $0 \leq u \leq U$. In any case, only *one* copy of the plane $\mathbb{E}_2$ is sufficient for the construction of the interior Green function.

On the other hand, for field and source points outside the grounded ellipse, such that $U \leq u_1, u_2 \leq \infty$, the Kelvin image is inside that ellipse, with $0 \leq 2U - u_2 \leq U$, only so long as the source is not too distant from the grounded ellipse. That is to say, the interior of the original grounded ellipse contains the image only for $u_2 \leq 2U$. But if the source is more distant, with $u_2 > 2U$, the chosen Kelvin image of the point source passes through the line

$R = \lim_{a\to 0} [a \cosh U|_{U=\ln(2R/a)} = \lim_{a\to 0} [a \sinh U|_{U=\ln(2R/a)}$. In this limit, only one copy of $\mathbb{E}_2$ is sufficient to solve either the interior or the exterior problem using the Kelvin method. See [6] for a thorough discussion of the grounded circular ring in 2D, where the standard Kelvin method is compared to the Sommerfeld method in considerable detail.

connecting the two foci and moves onto a *second* copy of $\mathbb{E}_2$ as also defined by (12) except with negative u. Therefore, for the point-like Kelvin image construction of the complete exterior Green function as expressed in (17), *two* copies of the real plane are required: One for $u > 0$ and another for $u < 0$. Effectively, the two elliptical foci on the x-axis at $x = \pm a$ are connected by a straight line segment that acts as a branch line "doorway"joining together these two copies of $\mathbb{E}_2$. So, to solve the exterior electric potential problem for a grounded ellipse, when real coordinates are used and point-like Kelvin images are located in an obvious way, a branched manifold is necessarily encountered. To put it another way, the actual, real interior of a grounded 2D elliptical conductor is insufficient to accommodate the location of a single point-like Kelvin image for an exterior point source, when that source is far from the conductor. More interior space is needed! All this is represented graphically in Figure 2

For the 3D embedding shown in that Figure, the surface has the appearance of being intrinsically curved, but that is an artefact of the parameterization. That part of the surface either above or below the blue line in Figure 2 corresponds to an open subset of $\mathbb{E}_2$. Those subsets of $\mathbb{E}_2$ follow immediately from a vertical projection of the surface shown onto the horizontal mid-plane of the Figure. This projection is shown explicitly in the second Figure of Appendix Appendix B:.

Another way to see these features for Kelvin images is through the use of conformal mapping. By mapping a circle onto an ellipse, the standard Kelvin image solution for a grounded circle is mapped onto an image solution for the grounded ellipse. (Please see Appendix Appendix B:.)

3.2 Mapping an infinite cylinder onto planes

What is at work here is the fact that G in (13) is really a Green function not just for the semi-infinite cylinder, with $u \geq 0$, but actually provides a solution to (14) for the infinite uv-cylinder, where $-\infty \leq u \leq +\infty$, along with $0 \leq v \leq 2\pi$. So no matter where the source is placed on that infinite cylinder, to construct G_o such that it vanishes at a fixed value of u, there is always room to accommodate a Kelvin point image. The only open issue is then how to map the infinite uv-cylinder onto one or more copies of the xy-plane. Sticking with the $x\,(u, v)$ and $y\,(u, v)$ relations in (12) gives a map that produces two copies of $\mathbb{E}_2$ as represented by the embedding shown in Figure 2 for the case $U = 3/2$. The original infinite uv-cylinder is flared out by the map onto x and y, both for large positive and for large negative u, but pinched down to a straight line segment connecting the foci at $x = \pm a$ when $u = 0$, with that segment situated "below" the grounded ellipse at $u = U$ ($= 3/2$ in the Figure). This is the geometry that underlies the Kelvin image method as applied here. The pinched line segment has some obviously singular geometric features, but these are not pathological.

On the other hand, there is another clear choice to map the infinite uv-cylinder onto planes that gives a different geometry. Rather than pinch the cylinder shut

in terms of x and y, at $u = 0$ or some other value of u, the cylinder may be folded around the location of the grounded ellipse so that the submanifold below the fold is just a "mirror image" of the submanifold above the fold. (Please see Figure 3.) This leads to the Sommerfeld image method which we describe in detail in the following. The fold also has some obviously singular geometric features, but again these are not pathological.

3.3 The Sommerfeld image method

Consider the same exterior Green function situation using Sommerfeld images. (The history of this alternate method is discussed in [9].) In this approach, the interior of the ellipse is eliminated, and two copies of the plane outside the grounded ellipse are joined together along the grounded ellipse.

The new parameterization of both copies of the xy-plane outside the ellipse with $u = U > 0$, again written in terms of real elliptic coordinates, is[7]

$$u = U + |w| \ , \tag{20}$$

$$x = a\cosh\left(U + |w|\right)\cos v, \quad y = a\sinh\left(U + |w|\right)\sin v, \tag{21}$$

$$-\infty \leq w \leq \infty, 0 \leq v \leq 2\pi.$$

So, when both field and source points are on the upper branch of the surface, such that $0 < w_1, w_2 < \infty$, a Green function is now given by

$$G\left(w_1, v_1; w_2, v_2\right) = -\frac{1}{4\pi}\left|w_1 - w_2\right| - \frac{1}{4\pi}\ln\left(1 + e^{-2|w_1 - w_2|} - 2e^{-|w_1 - w_2|}\cos\left(v_1 - v_2\right)\right). \tag{22}$$

But when the field point is on the upper branch and the source is on the lower branch, albeit with the same convention $0 < w_1, w_2 < \infty$, the corresponding Green function is

$$G\left(w_1, v_1; -w_2, v_2\right) = -\frac{1}{4\pi}\left(w_1 + w_2\right) - \frac{1}{4\pi}\ln\left(1 + e^{-2(w_1 + w_2)} - 2e^{-(w_1 + w_2)}\cos\left(v_1 - v_2\right)\right). \tag{23}$$

In this approach an exterior Green function for a grounded ellipse is the linear combination

[7] If the apparent du/dw slope discontinuity causes anxiety on the part of the reader, one may take instead $u\left(w\right) = \left(\sqrt{\left(U^2\right)^p + \left(w^2\right)^p}\right)^{1/p}$ for $p > 1/2$, again with $-\infty \leq w \leq \infty$. For example, see [6]. However, the ensuing complications in expressions involving Green functions are not worth making this generalization here, in our opinion.

$$
\begin{aligned}
G_o(w_1, v_1; w_2, v_2) &= G\left(w_1, v_1; w_2, v_2\right) - G\left(w_1, v_1; -w_2, v_2\right) \\
&= -\frac{1}{4\pi}\left|w_1 - w_2\right| + \frac{1}{4\pi}\left(w_1 + w_2\right) \\
&- \frac{1}{4\pi}\ln\left(1 + e^{-2|w_1 - w_2|} - 2e^{-|w_1 - w_2|}\cos\left(v_1 - v_2\right)\right) \\
&+ \frac{1}{4\pi}\ln\left(1 + e^{-2(w_1 + w_2)} - 2e^{-(w_1 + w_2)}\cos\left(v_1 - v_2\right)\right), \qquad (24)
\end{aligned}
$$

assuming that both field and source points are on the upper branch, i.e. $0 \leq w_1, w_2 \leq \infty$. Otherwise, $G\left(w_1, v_1; w_2, v_2\right) = G\left(w_2, v_2; w_1, v_1\right)$ and $G_o\left(-w_1, v_1; w_2, v_2\right) = -G_o\left(w_1, v_1; w_2, v_2\right)$. Consequently, this Green function again satisfies homogeneous Dirichlet boundary conditions on the ellipse, i.e. $G_o\left(0, v_1; w_2, v_2\right) = 0$ for all v_1, w_2, and v_2. And yet again, as in our previous discussion of the Kelvin method, G_o satisfies homogeneous Neumann boundary conditions at infinity, i.e. $\lim_{r\to\infty} \overrightarrow{\nabla} G_o = 0$.

Remarkably, as the reader may readily verify, the expressions (17) and (24) give exactly the same functions on the xy-plane when both field point (x_1, y_1) and

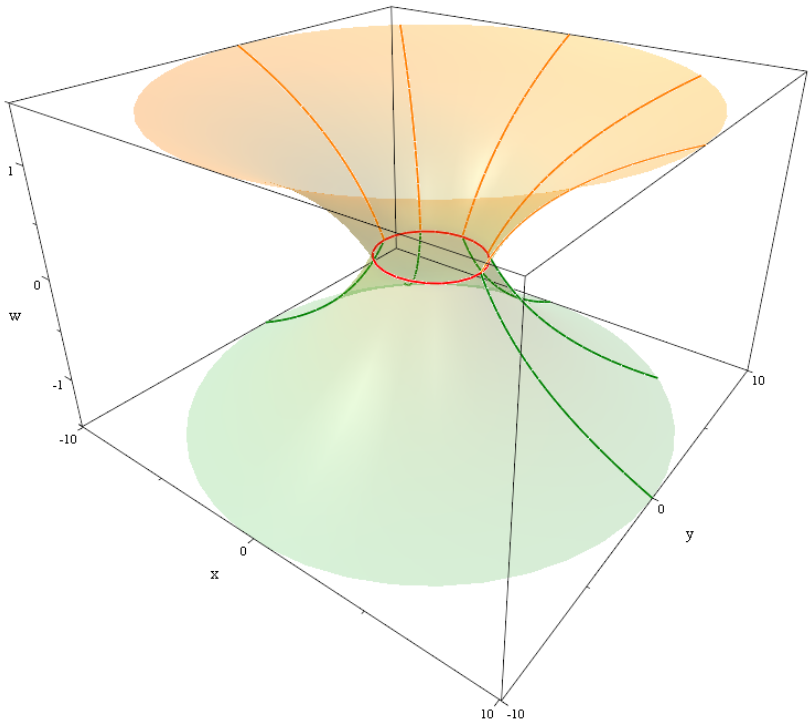

Figure 3. Representative trajectories for exterior sources (orange) and their Sommerfeld images (green) for a grounded ellipse (red), again with $U = 3/2$. All (x, y) points inside the red ellipse are excluded from the 2D manifold in this method.

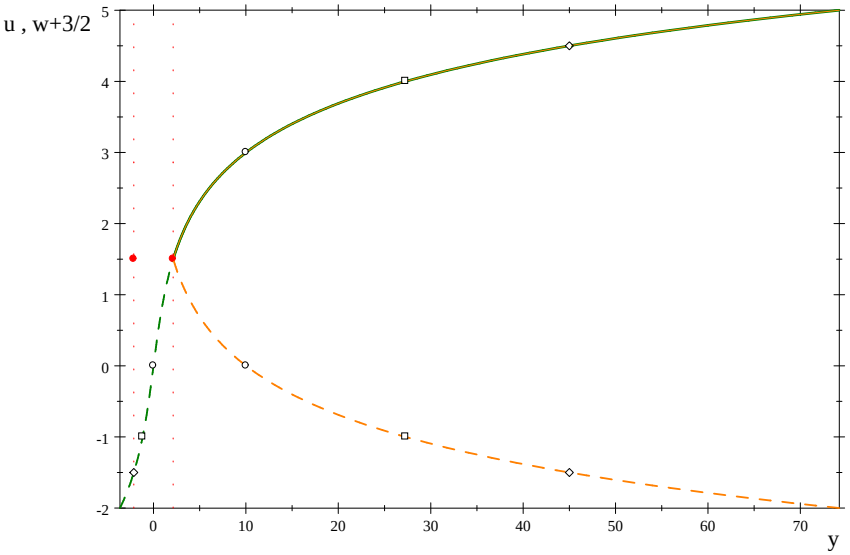

Figure 4. Source and image domains for $x = 0$, as solid and dashed curves, respectively.

source point (x_2, y_2) are located outside the grounded ellipse and on the upper $\mathbb{E}_2$ branch, despite the differences in the Kelvin and Sommerfeld image locations as evident upon comparing Figure 2 with the following Figure 3.

As in the previous Figure 2, the 3D embedding shown in Figure 3 has the appearance of being intrinsically curved, but that is again an artefact of the parameterization. That part of the surface either above or below the red ellipse in Figure 3 corresponds to an open subset of $\mathbb{E}_2$. Those subsets of $\mathbb{E}_2$ follow immediately from a vertical projection of the surface shown onto the horizontal mid-plane of the Figure, to obtain diagrams similar to those shown in Appendix Appendix B:.

Visualization of the features in these 3D Figures – especially their differences – may be easier if 2D vertical slices are considered. In Figure 4, the source and image domains along the y-axis are shown in green for the Kelvin method and in orange for the Sommerfeld method. Particular choices for point sources and their images are shown as small circles, squares, or diamonds, for an ellipse whose $x = 0$ points are shown in red. The source domain is always the same – namely, the planar region outside the grounded ellipse – no matter what image method is under consideration, so the orange and green curves in the Figure are the same for $u > 3/2$ or $w > 0$.

In Figure 5, the source and image domains along the x-axis are shown in green for the Kelvin method and in orange for the Sommerfeld method. As before, particular choices for point sources and their images are shown as small circles, squares, or diamonds, and the $y = 0$ points on the ellipse are shown in red. Once

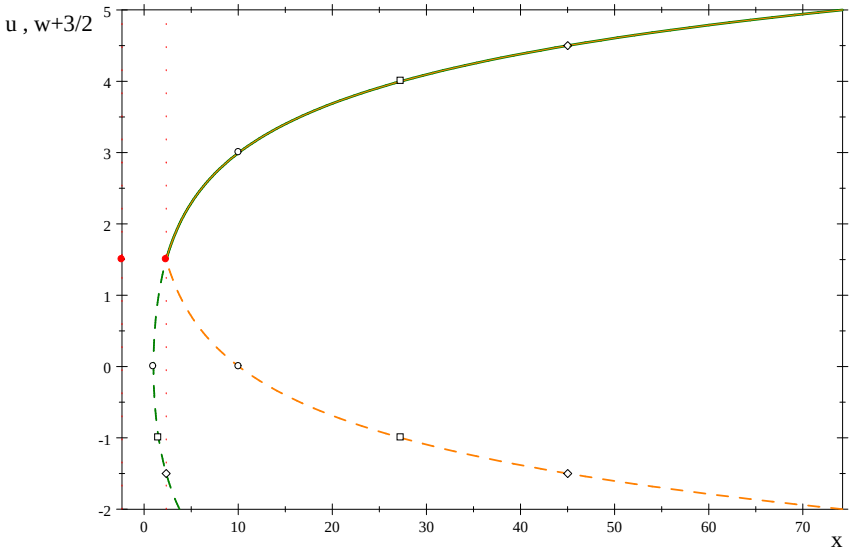

Figure 5. Source and image domains for $y = 0$, as solid and dashed curves, respectively.

again, the source domain is always the same no matter what image method is under consideration, but the image domains differ, depending on how the manifold is extended beyond the source domain.

4 Induced Charge Density

The actual linear charge density induced on the grounded ellipse is proportional to the normal component of the electric field evaluated in the limit where the field point approaches the ellipse. It suffices to consider the density induced by a unit point source outside the ellipse. Then the relevant normal electric field is just $-\partial G_o/\partial u_1|_{u_1=U}$ for the Kelvin image method, or $-\partial G_o/\partial w_1|_{w_1=0}$ for the Sommerfeld image method. The results are the same, using either method. The situation of interest for the external problem involves a unit source at $u_2 > U$ or $w_2 > 0$. In terms of the result for the Sommerfeld method, (24), we find the linear charge density

$$\begin{aligned}\lambda(v_1; w_2, v_2) &= -\frac{\partial}{\partial w_1} G_o\left(w_1, v_1; w_2, v_2\right)\Big|_{w_1=0, w_2>0} \\ &= \frac{1}{2\pi}\frac{e^{-2w_2}-1}{e^{-2w_2}-2e^{-w_2}\cos\left(v_1-v_2\right)+1}. \end{aligned} \tag{25}$$

Note that the total charge induced by a $+1$ source is always -1,

$$\int_0^{2\pi} \lambda\,(v_1; w_2, v_2)\, dv_1 = -1, \tag{26}$$

even if the unit source is removed to infinity.[8] In that infinite limit, the induced charge density becomes constant around the ellipse.

$$\lambda\,(v_1; w_2, v_2) \underset{w_2 \to \infty}{\sim} -\frac{1}{2\pi}. \tag{27}$$

Plots of the charge density for various selected source distances from the grounded ellipse are straightforward to produce and evince all the expected features when expressed in terms of our chosen elliptic coordinates, as illustrated in Figure 6.

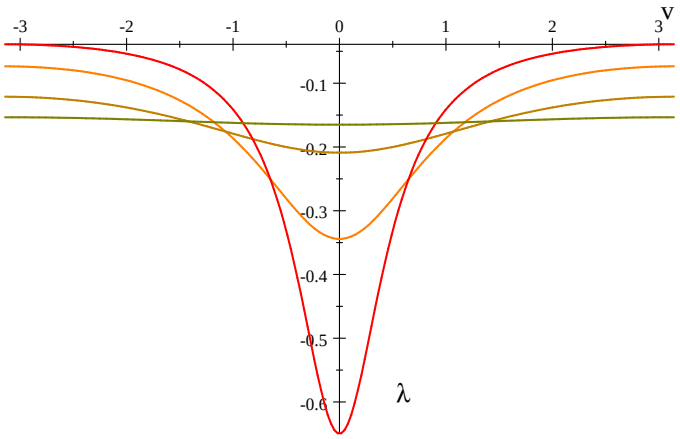

Figure 6. λ as a function of $v = v_1 - v_2$ for various w_2. Specifically, $w_2 = 1/2$ red, $w_2 = 1$ orange, $w_2 = 2$ sienna, $w_2 = 4$ brown.

5 A Straight Line Limit

A straight line limit of the ellipse is achieved by first setting $v = \pi/2$ in (12) so that $x \equiv 0$, and then letting $a \to \infty$ and $u \to 0$ so that $\lim_{a\to\infty, u\to 0}(a \sinh u) = y$ remains finite. The essential idea is that as $a \to \infty$ the elliptical (u, v) coordinates near the center of the x-axis become just rectangular Cartesian coordinates, (x, y). This behavior is evident in Figure 1 above, even for finite a.

[8] This is a peculiarity of the long-range Coulomb potential in 2D – it's logarithmic! In 3D the charge induced on a grounded ellipsoid by a unit source outside the sphere is not always -1, and in fact falls to zero as the source is removed to infinity [10, 11]. For a grounded hyper-sphere in N spatial dimensions, it is an interesting exercise to show the induced charge falls as a function of the source distance like r^{2-N} [8].

That is to say, let $u = y/a$ as $a \to \infty$ so that

$$a \sinh u \to ay/a = y. \tag{28}$$

At the same time, let $U = Y/a$ for $v = \pi/2$. Then $y\,(U, \pi/2) \to Y$ as $a \to \infty$. In this limit the Green functions (13) and (17) for similarly restricted us and vs are given by

$$\begin{aligned} G(u_1 = y_1/a, &v_1 = \pi/2; u_2 = y_2/a, v_2 = \pi/2) \\ &= -\frac{1}{4\pi a}|y_1 - y_2| - \frac{1}{4\pi}\ln(1 + e^{-2|y_1-y_2|/a} - 2e^{-|y_1-y_2|/a}) \\ &\underset{a\to\infty}{\sim} -\frac{1}{2\pi}\ln(|y_1 - y_2|/a) + O\Big(\frac{1}{a}\Big), \end{aligned} \tag{29}$$

$$\begin{aligned} G_o\,(u_1 = y_1/a, &v_1 = \pi/2; u_2 = y_2/a, v_2 = \pi/2) \\ &\underset{a\to\infty}{\sim} -\frac{1}{2\pi}\ln\left(\frac{|y_1 - y_2|}{|y_1 - 2Y + y_2|}\right) + O\left(\frac{1}{a}\right). \end{aligned} \tag{30}$$

Finally then,

$$\begin{aligned} \lim_{a\to\infty} G_o\,(u_1 = y_1/a, &v_1 = \pi/2; u_2 = y_2/a, v_2 = \pi/2) \\ &= -\frac{1}{2\pi}\ln\left(\frac{|y_1 - y_2|}{|y_1 + y_2 - 2Y|}\right). \end{aligned} \tag{31}$$

But for $y_1 > Y$ and $y_2 > Y$, this is precisely the 2D Green function at field point $(0, y_1)$ for a grounded straight line parallel to the x-axis, passing through the point $(x, y) = (0, Y)$, as obtained by placing at the point $(0, 2Y - y_2)$ a single negative Kelvin point image of a unit point source placed at position $(0, y_2)$. Of course, in this straight line limit where $x_1 = x_2$ the system is translationally invariant with respect to x, so there is no x dependence in the final Green functions.

When $x_1 \neq x_2$ but both are fixed and small, while a becomes infinite, a similar but slightly more tedious limit calculation gives the 2D Green function on the grounded half-plane, namely,

$$G_{\text{half-plane}}(x_1, y_1; x_2, y_2) = -\frac{1}{2\pi}\ln\left(\frac{\sqrt{(x_1-x_2)^2+(y_1-y_2)^2}}{\sqrt{(x_1-x_2)^2+(y_1+y_2-2Y)^2}}\right). \tag{32}$$

Once again, translational invariance with respect to x accounts for the dependence on only the difference, $x_1 - x_2$. We leave the detailed derivation of $G_{\text{half-plane}}$ from G_o for the ellipse as an exercise for the reader.[9]

[9] Results given in Appendix Appendix A: may be helpful.

6 Discussion

The standard problems involving a grounded circular ring in 2D [6] or grounded spheres in higher dimensions [8] can also be easily solved using either the Kelvin or Sommerfeld methods. However, there are many problems where the Kelvin method is very difficult, if not impossible, to implement, but which are directly solvable by the Sommerfeld method. Grounded semi-infinite planes and the circular disk in 3D Euclidean space provide well-studied examples [2, 7, 12–15].

Beyond these previously solved examples, the grounded ellipsoid in 3D and hyper-ellipsoids in higher dimensions are difficult problems that should be more tractable using Sommerfeld images. Existing image methods applied to these problems are quite involved, and usually require detailed properties of ellipsoidal harmonics [16]. In fact, extant treatments of the exterior 3D Green function problem for grounded ellipsoids use, in addition to an interior point image, a *continuous* distribution of Kelvin image charge on the surface of an interior confocal ellipsoid [10, 11] (also see Sections 7.4.3 and 7.4.4 in [16]). This non-trivial array of image charges results from requiring that all such charges reside entirely within the physical interior of the ellipsoid, *without* invoking a second copy of $\mathbb{E}_3$.

In contrast, the Sommerfeld method applied to a grounded ellipsoid embedded in N Euclidean dimensions only requires a single point image of the point source, in complete parallel to the grounded 2D ellipse treated here, albeit at the cost of introducing a second copy of $\mathbb{E}_N$. Therefore, in principle the Sommerfeld method should simplify the analysis required to construct Green functions for such ellipsoids, both conceptually and practically.

Acknowledgements

It has been our pleasure to reconsider this elementary subject during the Sommerfeld Sesquicentennial year. This work was supported in part by a University of Miami Cooper Fellowship and by a Clark Way Harrison Visiting Professorship at Washington University in Saint Louis.

Appendix A: Complex variables

Let

$$x + iy = a\left(\cos v \cosh u + i \sin v \sinh u\right) = a \cosh\left(u + iv\right). \tag{A1}$$

That is to say, $u + iv = \pm \operatorname{arccosh}\left(\frac{x+iy}{a}\right) + 2i\pi k \mid k \in \mathbb{Z}$. Choose the $+$ solution with $k = 0$ so that

$$u = \operatorname{Re}\left(\operatorname{arccosh}\left(\frac{x+iy}{a}\right)\right), v = \operatorname{Im}\left(\operatorname{arccosh}\left(\frac{x+iy}{a}\right)\right). \tag{A2}$$

Then find

$$r^2 = x^2 + y^2 = a^2(\cosh^2 u \cos^2 v + \sinh^2 u \sin^2 v)$$
$$= \frac{1}{2}a^2(\cosh 2u + \cos 2v) = a^2 \operatorname{arccosh}\left(\frac{x+iy}{a}\right) \operatorname{arccosh}\left(\frac{x-iy}{a}\right), \quad \text{(A3)}$$

as well as

$$x^2 - y^2 = a^2(\cosh^2 u \cos^2 v - \sinh^2 u \sin^2 v) = \frac{1}{2}a^2(\cosh 2u \cos 2v + 1), \quad \text{(A4)}$$

$$xy = a^2 \cosh u \cos v \sinh u \sin v = \frac{1}{4}a^2 \sinh 2u \sin 2v. \quad \text{(A5)}$$

In addition find

$$\sinh^2 2u = \frac{1}{2}\cosh 4u - \frac{1}{2}$$
$$= \frac{2}{a^4}\left(x^2 + y^2\right)^2 + \frac{2}{a^2}\left(y^2 - x^2\right)$$
$$+ \frac{2}{a^4}\left(x^2 + y^2\right)\sqrt{\left((x-a)^2 + y^2\right)\left((x+a)^2 + y^2\right)}, \quad \text{(A6)}$$

along with

$$v = \arccos\left(\frac{x/a}{\cosh u}\right) = \arcsin\left(\frac{y/a}{\sinh u}\right). \quad \text{(A7)}$$

Appendix B: Circle $\longleftrightarrow$ ellipse conformal mapping

Define a standard ellipse and its fiducial circle by

$$\frac{x^2}{a^2} + \frac{y^2}{b^2} = 1, \quad X^2 + Y^2 = \left(\frac{a+b}{2}\right)^2 \quad \text{(B1)}$$

Then circles in the complex $Z = X + iY$ plane are mapped to ellipses in the complex $z = x + iy$ plane, and vice versa, by [17]

$$z = Z + \frac{c^2}{4Z}, \quad c^2 = a^2 - b^2, \quad \text{(B2)}$$

By definition for any circle in the Z plane, $R^2 = \left(X^2 + Y^2\right) = |Z|^2$. Expressing R^2 in terms of x and y as given by the map (B2) then leads to

$$1 = \frac{R^2}{\left(R^2 + \frac{1}{4}c^2\right)^2}\, x^2 + \frac{R^2}{\left(R^2 - \frac{1}{4}c^2\right)^2}\, y^2 \quad \text{(B3)}$$

This is indeed another ellipse, confocal with the standard ellipse, only now with

$$a^2 = R^2\left(1 + \frac{c^2}{4R^2}\right)^2, \quad b^2 = R^2\left(1 - \frac{c^2}{4R^2}\right)^2, \quad a^2 - b^2 = c^2. \quad \text{(B4)}$$

The point is, concentric circles centered on the origin of the Z-plane are mapped by (B2) to confocal ellipses centered on the origin of the z-plane, and vice versa. Moreover, it is obvious and well-known [17] that the $Z \to z$ map actually covers the complex z-plane twice: Both the interior and the exterior of the fiducial circle cover the z-plane under the map.

But now consider the well-known electrostatics method to ground a circle by placing an image charge at a point obtained by inversion of the source location with respect to that grounded circle. Where does the conformal map (B2) take a point Z after it has been inverted with respect to the circle of radius $\frac{1}{2}(a+b)$? The effect of the inversion is

$$X \to \widetilde{X} = \Big(\frac{a+b}{2}\Big)^2 \frac{X}{R^2}, \quad Y \to \widetilde{Y} = \Big(\frac{a+b}{2}\Big)^2 \frac{Y}{R^2}. \tag{B5}$$

That is to say,

$$\widetilde{R}^2 = \widetilde{X}^2 + \widetilde{Y}^2 = \left(\frac{a+b}{2}\right)^4 \frac{1}{R^2}, \quad \widetilde{Z} = \widetilde{X} + i\widetilde{Y} = \frac{1}{R^2}\left(\frac{a+b}{2}\right)^2 Z. \tag{B6}$$

So then, the conformal map of this inverted point gives

$$\widetilde{z} = \widetilde{Z} + \frac{c^2}{4\widetilde{Z}} = \frac{1}{R^2}\Big(\frac{a+b}{2}\Big)^2 \left(Z + \frac{c^2}{\frac{4}{R^4}\Big(\frac{a+b}{2}\Big)^4 Z}\right) \tag{B7}$$

For example, suppose $a = 3$ and $b = 1$, then $(a+b)/2 = 2$ and $c^2 = 8$. Then

$$\begin{aligned} x &= \Big(1 + \frac{c^2}{4R^2}\Big)X\,, \quad y = \Big(1 - \frac{c^2}{4R^2}\Big)Y\,, \\ \widetilde{x} &= \Big(1 + \frac{c^2}{4\widetilde{R}^2}\Big)\widetilde{X}\,, \quad \widetilde{y} = \Big(1 - \frac{c^2}{4\widetilde{R}^2}\Big)\widetilde{Y}\,, \\ \widetilde{X} &= \Big(\frac{a+b}{2}\Big)^2 \frac{X}{R^2}\,, \quad \widetilde{Y} = \Big(\frac{a+b}{2}\Big)^2 \frac{Y}{R^2}\,. \end{aligned} \tag{B8}$$

More specifically, consider

$$\begin{aligned} (\widetilde{X}, \widetilde{Y})\big|_{a=b=2, X=2.5\cos\theta, Y=2.5\sin\theta} &= \Big(2^2 \times \frac{1}{2.5}\cos\theta, 2^2 \times \frac{1}{2.5}\sin\theta\Big) \\ (\widetilde{x}, \widetilde{y})\big|_{a=b=2, X=2.5\cos\theta, Y=2.5\sin\theta} &= \left(\left(1 + \frac{8}{4\Big(\frac{2^2}{2.5}\Big)^2}\right)2^2 \times \frac{1}{2.5}\cos\theta,\right. \\ &\qquad \left.\left(1 - \frac{8}{4\Big(\frac{2^2}{2.5}\Big)^2}\right)2^2 \times \frac{1}{2.5}\sin\theta\right). \end{aligned} \tag{B9}$$

For other points, see Figures B1 and B2. Upon comparing these two Figures, the various curves are related by the map (B2). Thus the solid or dashed circles

shown in Figure B1 map to the solid or dashed ellipses of the same color shown in Figure B2, and vice versa. Also, the light gray straight radial line in Figure B1 maps to the light gray hyperbolic curve in Figure B2, and similarly for other such radial lines.

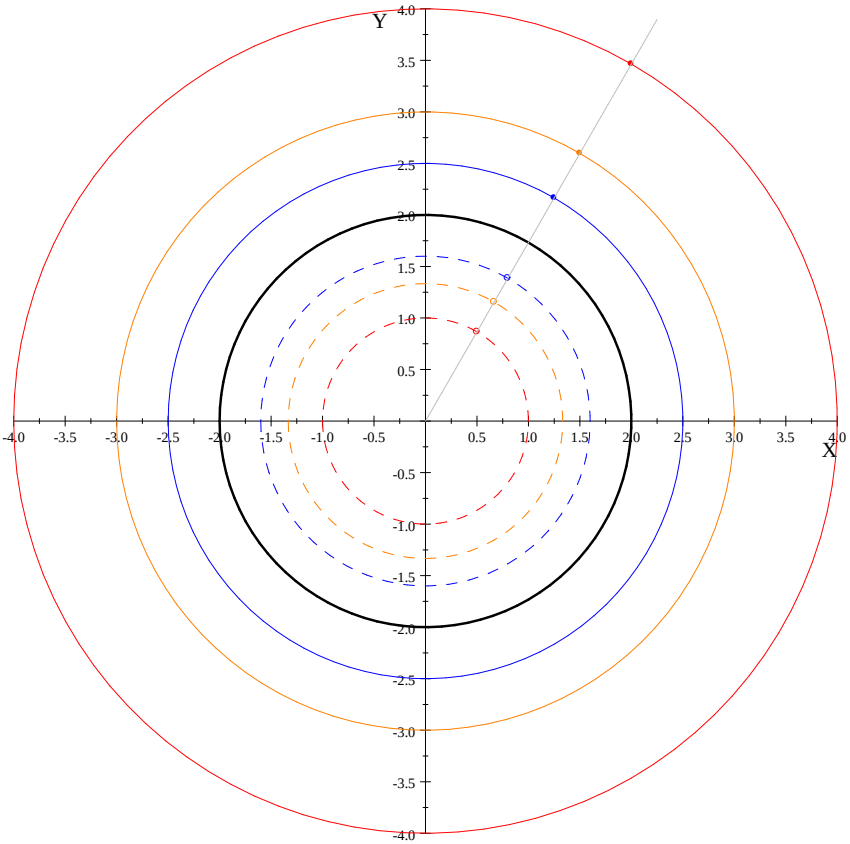

Figure B1. Various source (solid color curves) and Kelvin image (dashed color curves) charge locations for a grounded circle (shown in black). For one-to-one point source $\leftrightarrow$ point image pairing, only one copy of the plane is needed.

These Figures reproduce and confirm the explanation in the text that made use of real variables, namely, two copies of the plane are required to ground the ellipse using a single point image for each point source. The image locations shown by the orange and red dashed curves in Figure B2 are actually on the second branch of the doubled plane.

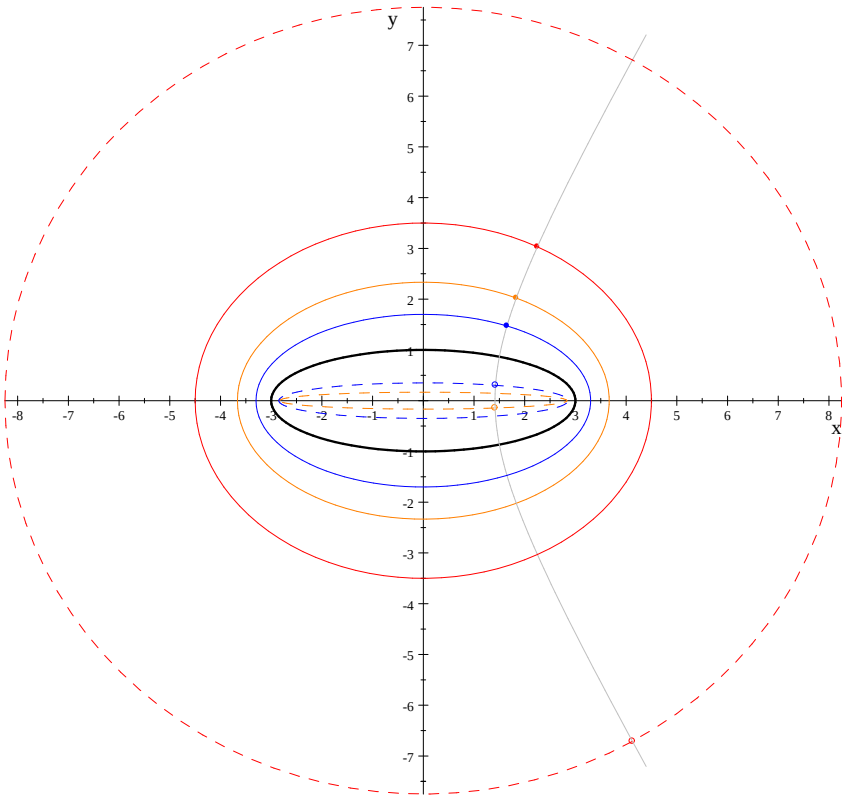

Figure B2. Various source (solid color curves) and Kelvin image (dashed color curves) charge locations for a grounded ellipse (shown in black). For one-to-one point source $\leftrightarrow$ point image pairing, two copies of the plane are now needed.

Appendix C: Contour plots of G_o

Consider the grounded ellipse defined by

$$(x,\, y) = (\cos(v)\cosh(1)\,,\ \sin(v)\sinh(1)) \quad \text{for} \quad 0 \le v \le 2\pi\,.$$

Three dimensional contour plots of $G_o \geq 0$, as functions of the field points on the xy-plane, are shown in the following Figures for three representative point source locations, with values near the point source truncated at $G_o = 0.25$. (For an animated version, with source locations varied for $0 \leq v \leq 2\pi$, please see this URL: http://www.physics.miami.edu/∼curtright/GoRotatingFigure.gif.)

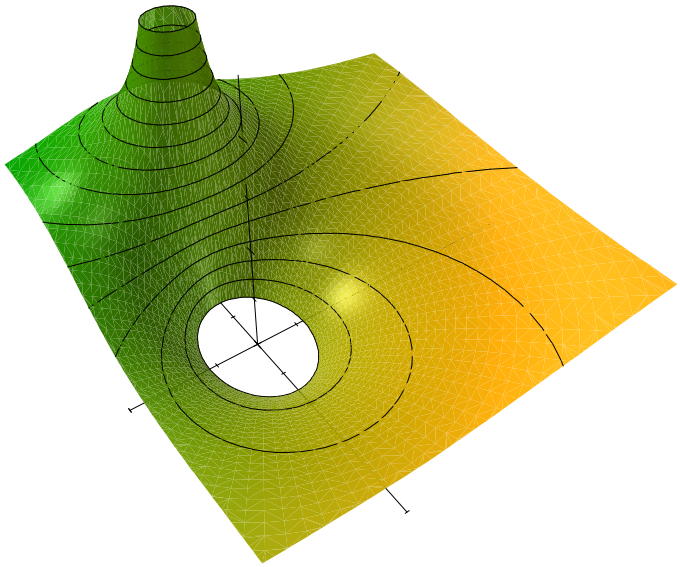

Figure C1. Contour plot of $G_o\,(x,y)$ with point source at $(x,y) = \left(\cos\left(\pi\right)\cosh\left(\frac{3}{2}\right), \sin\left(\pi\right)\sinh\left(\frac{3}{2}\right)\right)$.

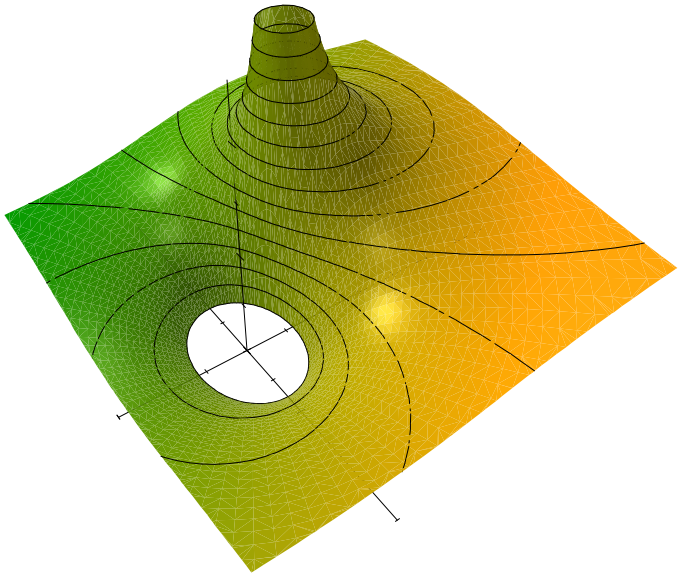

Figure C2. Contour plot of $G_o(x,y)$ with point source at $(x,y) = \left(\cos\left(\frac{2}{3}\pi\right)\cosh\left(\frac{3}{2}\right), \sin\left(\frac{2}{3}\pi\right)\sinh\left(\frac{3}{2}\right)\right)$.

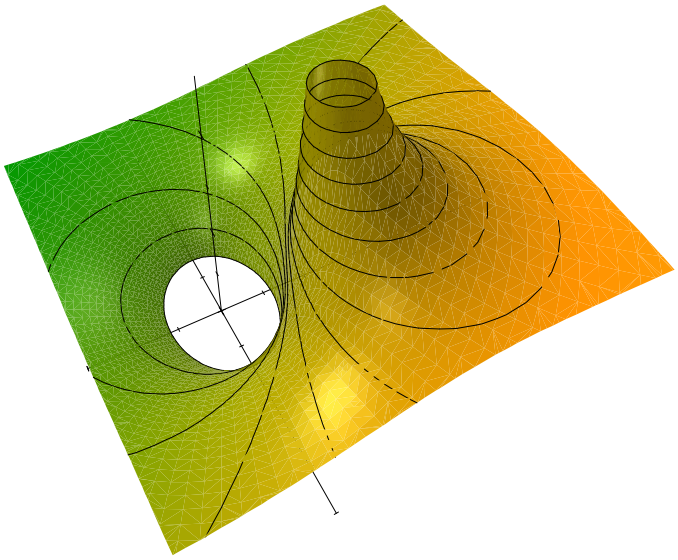

Figure C3. Contour plot of $G_o\left(x,y\right)$ with point source at $(x,y)=\left(\cos\left(\frac{1}{3}\pi\right)\cosh\left(\frac{3}{2}\right),\sin\left(\frac{1}{3}\pi\right)\sinh\left(\frac{3}{2}\right)\right)$.

References

[1] W. Thomson and P.G. Tait, *Treatise on Natural Philosophy*, Part I & Part II, Cambridge University Press (1879 & 1883).

[2] A. Sommerfeld, "Über verzweigte Potentiale im Raum"Proc. London Math. Soc. (1896) s1-28 (1): 395-429; ibid. 30 (1899) 161.

[3] G. Green, *An Essay on the Application of Mathematical Analysis to the Theories of Electricity and Magnetism*, Nottingham (1828).

[4] C. Neumann, "Ueber die Integration der partiellen Differentialgleichung: $\frac{\partial^2\Phi}{\partial x^2}+\frac{\partial^2\Phi}{\partial y^2}=0$"J. Reine Angew. Math. 59 (1861) 335-366, and *Untersuchungen über das logarithmische und Newton'sche Potential*, B G Teubner, Leipzig (1877).

[5] T.L. Curtright, N.M. Aden, X. Chen, M.J. Haddad, S. Karayev, D.B. Khadka, and J. Li, "Charged line segments and ellipsoidal equipotentials"Eur. J. Phys. 37 (2016) 035201, arXiv:1601.04047 [physics.class-ph].

[6] T. Curtright, H. Alshal, P. Baral, S. Huang, J. Liu, K. Tamang, X. Zhang, and Y. Zhang, "The Conducting Ring Viewed as a Wormhole"Eur. J. Phys. 40 (2019) 015206, arXiv:1805.11147 [physics.class-ph].

[7] D.G. Duffy, *Green's Functions with Applications*, Second Edition, CRC Press (2017) ISBN-13: 978-1482251029.

[8] H. Alshal and T. Curtright, "Grounded Hyperspheres as Squashed Wormholes"J. Math. Phys. 60 (2019) 032901, arXiv:1806.03762 [physics.class-ph].

[9] M. Eckert, *Arnold Sommerfeld: Science, Life and Turbulent Times 1868-1951*, Springer-Verlag (2013) ISBN-13: 978-1461474609.

[10] G. Dassios, "Directional dependent Green's function and Kelvin images"Arch. Appl. Mech. 82 (2012) 1325–1335.

[11] C. Xue and S. Deng, "Green's function and image system for the Laplace operator in the prolate spheroidal geometry" AIP Advances 7 (2017) 015024.

[12] E.W. Hobson, "On Green's function for a circular disc, with application to electrostatic problems"Trans. Cambridge Philos. Soc. 18 (1900) 277- 291.

[13] L. Waldmann, "Zwei Anwendungen der Sommerfeld'schen Methode der verzweigten Potentiale"Physikalische Zeitscrift 38 (1937) 654–663

[14] L.C. Davis and J.R. Reitz, "Solution to potential problems near a conducting semi-infinite sheet or conducting disc" Am. J. Phys. 39 (1971) 1255-1265.

[15] L.C. Davis and J.R. Reitz, "Solution of potential problems near the corner of a conductor"J. Math. Phys. 16 (1975) 1219–1226.

[16] G. Dassios, *Ellipsoidal Harmonics*, Cambridge University Press (2013) ISBN-13: 978-0521113090.

[17] Z Nehari, *Conformal Mapping,* Dover Publications (2011), especially pp 269-271, Eqn(4) et seq.